Intramolecular Dynamics of Dendrimers under Excluded-Volume Conditions

Fabio Ganazzoli,*,† Roberto La Ferla,‡ and Giuseppina Raffaini†

Dipartimento di Chimica, Politecnico di Milano, via L. Mancinelli 7, I-20131 Milano, Italy; and Research & Development, Bracco SpA, via E. Folli 50, I-20134 Milano, Italy

Received September 19, 2000; Revised Manuscript Received January 25, 2001

ABSTRACT: The dilute-solution dynamical properties of dendrimers in a good solvent are derived in the framework of the Rouse−Zimm approach. On the basis of a normal-coordinates treatment with preaveraged hydrodynamic interaction, we obtain the spectrum of relaxation times and some dynamical observables such as the viscoelastic complex modulus and the dynamic structure factor with its first cumulant. Since the latter quantity can also be calculated without preaveraging the hydrodynamic interaction, we can assess the accuracy of this approximation. The effect of both the structural symmetry and of the excluded-volume interactions on the intramolecular dynamics is discussed and the qualitative similarities with the effect of local stiffness are pointed out.

Introduction

Recently, there has been a great interest in hyperbranched molecules, particularly in dendrimers, that show a highly congested structure.[1,2] Recent synthetic procedures[3] have provided an almost perfect control of the architecture of these molecules, which stimulated a lot of experimental and theoretical work. Dendrimers may be described as formed by concentric layers defined by the branch points at the same topological distance from the core, with a molar mass that increases geometrically with the number of layers. The outermost layer also denotes the dendrimer generation.

The potential importance of such molecules is due both to their conformational properties and to their dynamical behavior.[1,2,4] Theoretical studies of dendrimer dynamics were typically carried out with analytical approaches ignoring topologically long-range interactions[5,6] (the excluded-volume problem) and with hybrid techniques using Monte Carlo simulations to obtain the instantaneous conformations that are required to correctly describe the hydrodynamic interaction.[7,8] Though computationally very demanding, simulation methods may easily account for long-range interactions and in principle do not require the preaveraging approximation common to analytical approaches. Unfortunately, in most cases, these studies were only concerned with the calculation of the intrinsic viscosity and not with intramolecular dynamics, apart from the work of one of us.[5]

The purpose of the present paper is to avoid the limitation of previous analytical approaches by studying the intramolecular dynamics of dendrimers in a good solvent within the Rouse−Zimm model.[9,10] In ref 4 (hereafter denoted also as paper I), we studied the good-solvent expansion of dendrimers mainly in terms of equilibrium properties, while the dynamical results were confined to the study of the viscometric radius obtained from intrinsic viscosity. Here we give a fuller account of the intramolecular dynamics, where the topological peculiarities of dendrimers are most relevant.

In the following, we first summarize our previous work about the good-solvent expansion and the solution of the dynamical eigenvalue problem that enabled us in paper I to calculate inter alia the intrinsic viscosity. Then we introduce the dynamical quantities of interest, namely the viscoelastic complex modulus, the dynamic structure factor, and its first cumulant. Afterward, we present the calculated viscoelastic relaxation spectrum, whose degeneracy is related to the statistical symmetry of the molecules, as discussed in the Appendix. Subsequently, we show our results for the dynamic quantities and for the static structure factor for a comparison. We also carry out a short comparison with previous theoretical results obtained by one of us[5] and by other authors neglecting good-solvent expansion. Finally, we summarize the main results of the present work pointing also out some analogies with those obtained for stiff models.

Mathematical Section

The theoretical study of dynamics within the usual Rouse−Zimm approach under good-solvent conditions was already outlined in paper I. Here, we briefly summarize our procedure, and provide the theoretical expressions of the quantities of interest. We consider dendrimers formed by f trees of order m (the dendra) connected to a central core and comprising P bonds between neighboring branch points. The molecular topology can be viewed as formed by a sequence of concentric layers. The outmost layer defines the dendrimer generation g, numbered from 0 (no branch point beyond the central core) onward. The total number of beads n is given by $n = 1 + fP(m^{g+1} - 1)/(m - 1)$. We report results for dendrimers with P equal to 1 or 2 having a ternary core ($f = 3$) and binary dendra ($m = 2$), so that each branch point is trifunctional. Sketches of these dendrimers, simply denoted as DP−Gg, are reported in paper I. In the conformational study we adopted freely jointed "bond" vectors of unit length connecting adjacent beads (subject to the excluded-volume interactions), while in dynamics we adopt the bead-and-spring model, a spring of unit mean-square length simply replacing each bond.

The good-solvent conformational properties of dendrimers were obtained in paper I by self-consistent minimization of the intramolecular free energy, accounting for the configurational entropy and for the

* To whom correspondence should be addressed.
† Politecnico di Milano. E-mail:fabio.ganazzoli@polimi.it. URL: http://dept.chem.polimi.it/home_page/ganazzoli.
‡ Bracco SpA. E-mail: rlaferla@bracco.it.

10.1021/ma001613z CCC: $20.00
Published on Web 05/03/2001

repulsive two-body interactions. The variational quantities were the average scalar products among the bond vectors. These scalar products yield the quadratic averages that describe the equilibrium state, such as the mean-square distances $\langle r_{ij}^2 \rangle$ among bead pairs i, j and the mean-square radius of gyration $\langle R_S^2 \rangle$. Moreover, they permit also calculation of the force-constant matrix **A** for any topology.[5,11,12] Within the Gaussian approximation, from the $\langle r_{ij}^2 \rangle$ values, we also get the elements of the matrix **H** embodying the preaveraged hydrodynamic interaction in partial-draining conditions. Following Zimm's approach,[9,10,13] the dynamical problem reduces to solving the eigenvalue equation[4,5]

$$[\mathbf{H}\cdot\mathbf{A}]\cdot\mathbf{Q} = \mathbf{Q}\cdot\Lambda \qquad \Lambda = \{\lambda_p\, \delta_{pq}\} \tag{1}$$

The diagonalization of the nonsymmetrical matrix $\mathbf{H}\cdot\mathbf{A}$ can be easily performed numerically.[5] The eigenvalue matrix Λ contains a zero eigenvalue related to the diffusion of the center of mass, and the relaxation rates of the normal modes of motion λ_p, $p = 1, 2, ..., n - 1$, which produce the viscoelastic relaxation times $\tau_p = (2\sigma\lambda_p)^{-1}$. Here $\sigma = 3k_BT/\zeta l^2$ is the time constant, ζ being the bead friction coefficient and l the bond length. The eigenvectors, collected in matrix **Q**, connect the column vector ξ of the normal coordinates ξ_p, $p = 0, 1, 2, ..., n - 1$, and the column vector **r** of the vector position of the beads $\mathbf{r}_i$, $i = 0, 1, 2, ..., n - 1$:

$$\mathbf{r} = \mathbf{Q}\cdot\xi \tag{2}$$

More details on the eigenvalue equation can be found in Appendix B of ref 5. We stress here that good-solvent expansion affects both the force-constant matrix **A** and the hydrodynamic-interaction matrix **H** in a nontrivial way.[5,14]

Through the eigenvalues and eigenvectors of $\mathbf{H}\cdot\mathbf{A}$, we can calculate various experimental quantities. The first one is the viscoelastic complex modulus $G(\omega) = G'(\omega) + iG''(\omega)$, measured under an oscillating shear deformation with an applied frequency ω. Its real and imaginary components, denoted also as elastic and loss moduli, are given by[9,10]

$$\mathrm{G}'(\omega) = \frac{RT}{M}\sum_{p=1}^{n-1}\frac{\bar{\omega}^2}{\bar{\omega}^2 + 4\lambda_p^{\,2}} \tag{3}$$

$$\mathrm{G}''(\omega) = \frac{2RT}{M}\sum_{p=1}^{n-1}\frac{\bar{\omega}\lambda_p}{\bar{\omega}^2 + 4\lambda_p^{\,2}} \tag{4}$$

where $\bar{\omega} = \omega/\sigma$ is the adimensional frequency. Note that in eq 4 the contribution of the solvent viscosity is already subtracted.

Another important quantity is the dynamic structure factor $S(q,t)$, measured in quasi-elastic scattering experiments. Here, q is the modulus of the scattering vector given by $q = |\mathbf{q}| = 4\pi\sin(\vartheta/2)/\lambda$, ϑ being the scattering angle and λ the wavelength of the radiation. $S(q,t)$ is obtained from the following expression:[10]

$$S(q,t) = n^{-2}\sum_j\sum_{k=0}^{n-1}\langle\exp\{-i\mathbf{q}\cdot[\mathbf{r}_k(t) - \mathbf{r}_j(0)]\}\rangle \tag{5}$$

In the assumption of a Gaussian distribution of $[\mathbf{r}_k(t) - \mathbf{r}_j(0)]$, after a minor change of the dummy indices, eq 5 can be written as

$$S(q,t) = n^{-2}\sum_i\sum_{j=0}^{n-1}\exp\left[-\frac{q^2}{6}\langle|\mathbf{r}_j(t) - \mathbf{r}_i(0)|^2\rangle\right] \tag{6}$$

$$= \exp[-q^2\,Dt]\,\frac{1}{n^2}\sum_i\sum_{j=0}^{n-1}\exp\left[-\frac{q^2}{6}\langle r_{ij}^{\,2}(t)\rangle\right]$$

Here, we separated the contribution of the zeroth mode, yielding the diffusion coefficient D, from that of the internal modes, which produce the time-dependent mean-square distances $\langle r_{ij}^2(t)\rangle$ irrespective of the position of the center of mass. In bond-length units we have

$$\langle r_{ij}^{\,2}(t)\rangle = \langle r_{ij}^{\,2}\rangle + 2\sum_{p=1}^{n-1} Q_{ip}Q_{jp}\mu_p^{\,-1}[1 - \exp(\sigma\lambda_p t)] \tag{7}$$

In this equation, μ_p are the diagonal elements of the μ matrix:

$$\mu = \mathbf{Q}^T\cdot\mathbf{A}\cdot\mathbf{Q} \qquad \mu = \{\mu_p\,\delta_{pq}\} \tag{8}$$

Upon setting $t = 0$ in eqs 5 and 6, we recover the static structure factor $S(q)$, known also as the form factor. Although not a dynamic quantity, we report it in the following because of some common features it shares with the first cumulant (see later).

The dynamic structure factor is often characterized through its first cumulant $\Omega(q)$, produced by the initial logarithmic slope:

$$\Omega(q) = -\frac{\partial}{\partial t}\ln\left(\frac{S(q,t)}{S(q,0)}\right)\Bigg|_{t\to 0} \tag{9}$$

The first cumulant is somewhat ill-defined because of the $t \to 0$ limit, when in principle the local relaxation within each monomer is important. While this problem does not arise when using coarse-grained models, the experimental time scales of the local and of the collective rearrangements usually differ by a few orders of magnitude, so that in practice they are easily separated in appropriate experiments. However, this may not be true in the case of very stiff polymers, where there is no clear distinction between the local and the collective dynamics.

Neglecting the local relaxation within the monomer, the first cumulant can be calculated as[15]

$$\Omega(q) = \frac{q^2l^2\sigma}{S(q)}\left[1 + \frac{\zeta_r}{n}\sum_i\sum_{j=0}^{n-1}(1 - \delta_{ij})\left\langle\frac{l}{r_{ij}}\right\rangle f(x_{ij})\right] \tag{10}$$

where $\zeta_r = \zeta/6\pi\eta_0 l$ is the reduced friction coefficient (here we put $\zeta_r = 0.25$),[12,14] η_0 being the solvent viscosity, and $\langle l/r_{ij}\rangle$ is obtained from $\langle r_{ij}^2\rangle$ in the Gaussian approximation. x_{ij} is the dimensionless variable $x_{ij} = q(\langle r_{ij}^2\rangle/6)^{1/2}$ and $f(x)$ is a function that may be calculated with or without preaveraging the hydrodynamic interaction:

$$f(x) = \begin{cases}\exp(-x^2) & \text{with preaveraging}\\ \frac{3}{4}(x^{-3} + x^{-1})e^{-x^2}\int_0^x e^{-t^2}dt - x^{-2} & \text{without preaveraging}\end{cases} \tag{11}$$

Therefore, computation of the first cumulant enables us

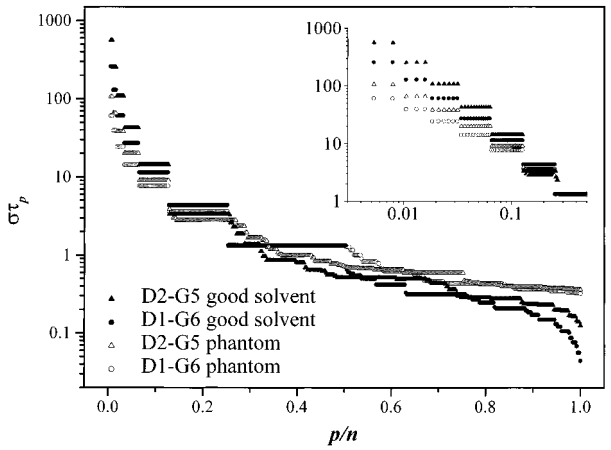

Figure 1. Spectrum of relaxation times $\tau_p = (2\sigma\lambda_p)^{-1}$ as a function of the mode index for D1−G6 (circles) and D2−G5 (triangles) dendrimers. Empty symbols are for the phantom model with a random-walk conformation; filled symbols apply to molecules with good-solvent expansion. The inset shows the same values in a doubly logarithmic plot for the collective modes (up to $p/n < 0.5$ for D1−G6 and $p/n < 0.25$ for D2−G5) to better show their multiplicity.

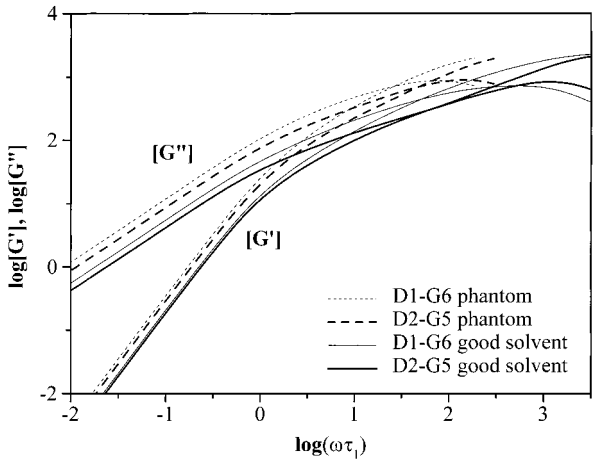

Figure 2. Real and imaginary part of the complex modulus in reduced units, [G'] and [G''] (see text), plotted as a function of the applied frequency ω, normalized by the longest relaxation time τ_1 for the largest-generation dendrimers under good-solvent conditions and in the phantom state.

to gauge the error entailed by the preaveraging approximation.

The numerical results reported in the following for D1 and D2 dendrimers apply to the same good-solvent conditions that were chosen in paper I for describing the intramolecular expansion and the generation dependence of the molecular size.[16] For a comparison, we also report results for the phantom dendrimers of both D1 and D2 families with a random-walk conformation.

Results and Discussion

Spectrum of the Relaxation Times. Before discussing the effect of good-solvent expansion on the relaxation times shown in Figure 1, we point out that an important feature consists of their multiplicity, strictly related to molecular symmetry. This multiplicity is already apparent in the semilogarithmic plot used in the figure, but it is best seen for the collective modes in the doubly logarithmic plot of the inset. Ignoring good-solvent expansion and hydrodynamic interaction, analytical theory can be carried out for the Rouse model[6] by setting $\mathbf{H} \equiv \mathrm{I}$ in eq 1 and taking $\mathbf{A}$ simply as the topological incidence matrix[5] (see also the Appendix). It turns out that there are $1 + (g + 1)P$ nondegenerate eigenvalues, $(g + 1)P$ subgroups of $(f - 1)$-degenerate eigenvalues and $(g - k)P$ subgroups of eigenvalues with degeneracy $fm^k(m - 1)$, $k = 0, 1, 2, ..., g - 1$ (in our case $f = 3$, $m = 2$). More details about the eigenvalues and the associated eigenvectors can be found in the Appendix. The first degenerate eigenvalues of each subgroup yield the relaxation times of the collective modes with $p/n < 0.5$ for D1 and $p/n < 0.25$ for D2 dendrimers reported in the inset of Figure 1. Inclusion either of hydrodynamic interaction or of good-solvent expansion does not remove the degeneracies, since these are dictated by molecular symmetry, but may slightly alter the ordering of the relaxation times of a few internal modes.

Good-solvent expansion enhances the breadth of the spectrum of the relaxation times compared to the phantom state, as shown in Figure 1 for D1−G6 and D2−G5 (the largest generations considered by us for the two families; note that these dendrimers roughly comprise the same number of beads). In particular, the relaxation times of the collective modes with $p/n < 0.5$ for D1 and $p/n < 0.25$ for D2 dendrimers become longer (see the inset of Figure 1), whereas those of localized modes become shorter. In other words, because of good-solvent expansion the molecules require a longer time to lose memory of their large-scale conformations, while the relaxation becomes faster on the local scale. Thus, at the largest generations (see Figure 1) the spectrum spans almost four decades in both families, instead of just above two as in the phantom molecules. Because of that, the intramolecular dynamics is better distinguished in large-generation dendrimers at a large expansion, whereas in phantom molecules we have a continuous crossover from the dynamics of the whole molecule to the dynamics of the single bead (see also later). Such good-solvent behavior is qualitatively similar to what is predicted for stiffer models. In fact, as pointed out in paper I, dendrimer expansion can be described as an outward stretching of the individual dendra, akin to the effect of a larger local stiffness. It should be remembered however that in general good-solvent expansion produces a nonaffine deformation of the molecule with topological long-range effects, so that in principle we cannot expect any quantitative correspondence with some appropriate freely rotating (i.e., stiff), but phantom, model.

Phantom dendrimers show a universal behavior of the relaxation times within each family (D1 or D2) when plotted as a function of p/n, p being the mode number. In principle, such universality is no more present under good-solvent expansion because of the nonaffine expansion of dendrimers. Still, and quite surprisingly, the differences are so small that in practice the above universality is still valid. Conversely, no universality exists between the two families, as shown by Figure 1. Thus, the collective modes of D2 dendrimers show longer relaxation times than either D1 dendrimers with roughly the same bead number (see for instance D2−G5 and D1−G6 in Figure 1) or *a fortiori* D1 dendrimers at the same g. In conclusion, a large density of branch points accelerates the intramolecular relaxation.

Complex Modulus. In Figure 2 we show the reduced elastic and loss moduli [G'] and [G''] calculated for dendrimers D1−G6 and D2−G5 as a function of the

normalized frequency $\omega\tau_1$, $\tau_1 = (2\sigma\lambda_1)^{-1}$ being the longest viscoelastic relaxation time. Here, we defined the reduced quantities $[G'] = G'M/RT$ and $[G''] = G''M/RT$ (see also eqs 3 and 4). For each family, lower generation dendrimers have smaller moduli, as reported in ref 5. At low-frequency we have the usual behavior, with $[G'] \propto \omega^2$ and $[G''] \propto \omega$, and $[G''] \gg [G']$, the molecules contributing only to the solution viscosity.

The increased breadth of the spectrum of relaxation times due to good-solvent expansion allows us to better recognize the region of intramolecular dynamics for the highest-generation dendrimers. This region is probed at frequencies $\omega\tau_1 > 1$, provided $\omega\tau_{n-1} < 1$, τ_1 and τ_{n-1} being the largest and the shortest relaxation times. Within this range, the two moduli have the same order of magnitude and for the largest g they roughly behave as in linear and star polymers, where $[G'] \propto (\omega\tau_1)^{\alpha_1}$ and $[G''] \propto (\omega\tau_1)^{\alpha_2}$. This behavior is most apparent in D2−G5 dendrimer, where we find $\alpha_1 = 0.55$ and $\alpha_2 = 0.46$ in good-solvent conditions (thick solid lines in Figure 2). In phantom molecules, similar power laws are harder to recognize, and we may tentatively extract the apparent exponents $\alpha_1 = 0.70$ and $\alpha_2 = 0.52$ (thick dashed lines in Figure 2). No power-law dependence can be recognized both in lower-generation and in D1 dendrimers.

In linear and star polymers, the α_1 and α_2 exponents are asymptotically equal, with $\alpha_1 \equiv \alpha_2 = \alpha = {}^2/_3$,[10,13] though for finite chains one finds $\alpha_1 \gtrsim \alpha_2$.[17] Here, α is related[10,13] to the exponent of the relaxation times $\tau_p \propto (p/n)^{-1/\alpha}$, and we have the familiar relationship $\tau_p \propto (n/p)^{3/2}$. Conversely, dendrimers do not show any power-law dependence from p/n, since their relaxation times show an exponentially fast decrease with increasing mode index, as seen also in Figure 1 even ignoring the degeneracies within each subgroup. This decrease of relaxation times for the collective modes is accompanied by an increasingly larger multiplicity, as said before, unlike what happens in linear and in star polymers: here, the multiplicity is fixed for a given mode parity, and at large arm number only the degenerate modes with $f - 1$ multiplicity do matter. As a consequence, dendrimers show a large mixing of the contribution of the individual modes, which does not produce any linear portion in a log−log plot of $[G']$ and $[G'']$, unless one considers the highest generations.

A further crossover in the elastic and loss moduli is present for $\omega\tau_{n-1} > 1$, where the coarse-grained bead-and-spring model produces the unphysical results of a maximum of $[G'']$ and a plateau of $[G']$. This additional model-dependent feature contributes to modify in most cases the apparent α exponent, which in conclusion has no general validity in dendrimers.

Static Structure Factor. Although not a dynamic quantity, we report here the static structure factor $S(q)$ of dendrimers in a good solvent for a comparison with the first cumulant (see later). Thus, in Figure 3 we report $S(q)$ for large-generation D1 and D2 dendrimers through a Kratky plot by showing $q^2\langle R_S^2\rangle S(q)$ as a function of $q\langle R_S^2\rangle^{1/2}$. Note that these reduced variables produce universal plots in the low-q range. The main feature of the plots in Figure 3 consists of a peak at an abscissa value around 2 that is present for molecules both in a good solvent and in the phantom state, the main differences being present at larger q values.

The Kratky plot is particularly useful to recognize the molecular shape and branching, but also to some extent the good-solvent expansion and/or the local stiffness.

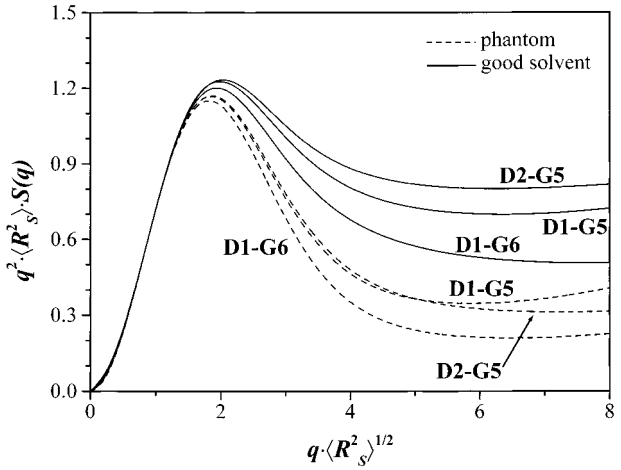

Figure 3. Static structure factor $S(q)$ plotted as $q^2\langle R_S^2\rangle S(q)$ vs $q\langle R_S^2\rangle^{1/2}$ (Kratky plot) for high-generation D1 and D2 dendrimers.

Accordingly, star polymers with at least four or five arms show a maximum in the Kratky plot at $q\langle R_S^2\rangle^{1/2} \gtrsim 2$, corresponding to a distance of observation somewhat smaller than the radius of gyration.[18] Such maximum, due to the increased monomer density near the star core because of the molecular topology, slowly shifts to a smaller abscissa, and becomes sharper and slightly lower, the larger is the number of arms. Qualitatively analogous results were obtained by one of us for dendrimers using a freely rotating model and neglecting good-solvent expansion:[5] from the 3rd generation onward, the Kratky plot shows an increasingly well-pronounced peak whose position slightly shifts to a lower abscissa with increasing g. Moreover, the curves do not show any indication of a secondary or higher order maximum, as expected for solid or hollow spheres.

Our present results, reported in Figure 3, qualitatively confirm the above findings concerning the peak position and sharpness, and therefore in the following we only stress the main differences between D1 and D2 dendrimers under good-solvent expansion and the phantom-molecule results, as done before. First of all, we note that in the latter case for $q\langle R_S^2\rangle^{1/2} \lesssim 4$ the Kratky plots of D1 and D2 dendrimers at the same g do essentially overlap (dashed curves for D1−G5 and D2−G5 in the phantom state in Figure 3). This means that within this range the scattered intensity is simply due to the overall topology and symmetry of the two dendrimer families in the phantom state. The different number of segments between adjacent branch points of D1 and D2 dendrimers affects the static structure factor only at larger q (with $q\langle R_S^2\rangle^{1/2} \gtrsim 5$). Furthermore, the larger is g, the larger is the $q\langle R_S^2\rangle^{1/2}$ value where this universality breaks down because of the larger radius of gyration. Conversely, no universality can be seen in the presence of good-solvent expansion, neither at a fixed generation g (compare the curves of D2−G5 with those of D1−G5), nor at the same number of beads (or nearly so) as seen by comparing D1−G6 and D2−G5 dendrimers in Figure 3. This is clearly due to the different expansion pattern of the two dendrimer families. A common feature due to good-solvent expansion resides in the increased broadness of the peaks, which may even disappear for $g = 2$, and in a minor shift of their position. Furthermore, the steady increase of $q^2\langle R_S^2\rangle S(q)$ at $q\langle R_S^2\rangle^{1/2}$ larger than $8 \div 10$ (not shown in Figure 3) is again consistent with a larger local stiffness because of good-

solvent expansion,[19] somewhat analogous to previous results for stiffer freely rotating models obtained by one of us.[5]

Monte Carlo simulations[20] predicted a similar pattern for the Kratky plot, with a pronounced maximum in the same position as we calculate, but also a secondary weak maximum roughly consistent with the expected pattern of a solid sphere. Another qualitative difference consists of the peak present for the $g = 1$ dendrimer (according to our results, a peak should appear in the Kratky plot only for $g \geq 2$), possibly related to the larger number of segments between adjacent branch points. Some experimental results were obtained with small-angle neutron scattering from poly(propyleneimine) dendrimers with a twin core,[21] a topology not identical to ours. These data do indeed show a peak at the predicted position in a Kratky plot, with some hints of a secondary maximum for $g = 4$ (our notation). Surprisingly, the main peak is present even for the molecule with $g = 0$ having a very small molecular size. Also, in all cases the curves fall steadily to zero after the peak, unlike what was predicted by us and obtained with Monte Carlo simulations.[20] More extensive results were obtained with small-angle X-ray scattering from poly(amidoamine) dendrimers, having a twin core and a generation comprised between 2 and 9, in our notation.[22] Unfortunately, these data were not reported in a Kratky plot, so that we cannot easily compare the position of the main peak. However, starting from the fifth generation onward the scattered intensities definitely showed one or more higher-order peaks, up to at least three in the case of $g = 9$, closely corresponding to the positions expected for a solid sphere. The failure of our calculations to reproduce such features for these congested dendrimers should be attributed to our use of the Gaussian approximation, which is basically adequate for most purposes,[23] but cannot produce any flat density profile such as is expected for a compact sphere.

Dynamic Structure Factor and Its First Cumulant. The dynamic structure factor turns out to be relatively ineffective per se to study the intramolecular dynamics of dendrimers because of the short length of the dendra. In fact, the intramolecular dynamics can be probed within appropriate q values as done before for the static structure factor, *and* within an appropriate time window (the reciprocal of the frequency window previously discussed for the complex modulus), being soon dominated by the fast diffusion of the whole molecule, related in turn to its small size. Accordingly, $S(q,t)$ shows only small deviations from the simple exponential characteristic of pure diffusion for all q values but the largest ones. In Figure 4 we show the dynamic structure factor of dendrimers D1−G6, D1−G5, and D2−G5 at $ql = 0.5$. Deviations from a simple exponential are evident in the two upmost curves, that apply to dendrimers D1−G6 and D2−G5 in a good solvent, but not for lower generations and for phantom molecules. As noted before, dendrimer expansion broadens the spectrum of relaxation times and increases the molecular size, thus making it easier to follow the intramolecular dynamics at relatively short times. In any case, the linearity of all the curves in Figure 4 at large times corresponds to the diffusion of the whole molecule.

The first cumulant $\Omega(q)$ is obtained from the initial slope of the above curves. This is the only dynamical quantity that may be easily evaluated both with and without preaveraging the hydrodynamic interaction, thus providing a useful tool to investigate the importance of this approximation, albeit within the Gaussian assumption (see after eq 10). $\Omega(q)$ is shown in Figure 5 as $\Omega(q)/\sigma(ql)^3$ vs $q\langle R_S^2\rangle^{1/2}$, which yields a universal plot in the low-q range as in the Kratky plot previously discussed. The normalization of the vertical axis arises

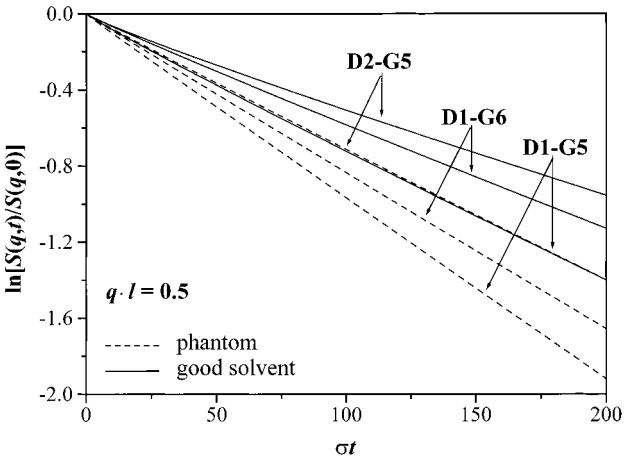

Figure 4. Dynamic structure factor $S(q,t)$ plotted as a function of time (in σ units, see text) at $ql = 0.5$ for the same dendrimers as in Figure 4.

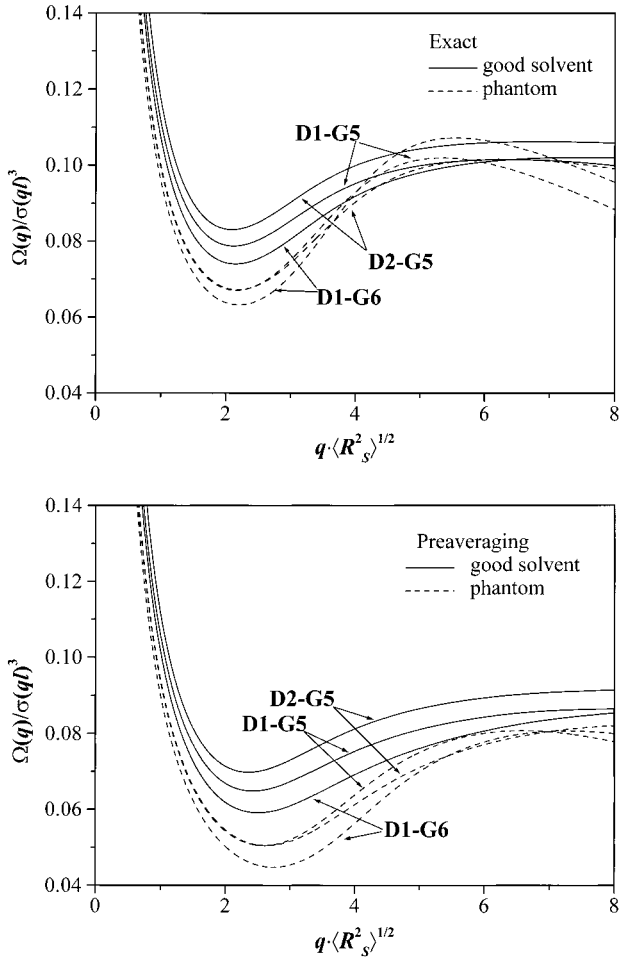

Figure 5. First cumulant of the dynamic structure factor plotted as $\Omega(q)/\sigma(ql)^3$ vs $q\langle R_S^2\rangle^{1/2}$ for the same dendrimers as in Figures 3 and 4. The "exact" result (no preaveraging of the hydrodynamic interaction, but still within the Gaussian approximation) is shown in the upper plot, and the preaveraged result is shown in the lower one.

from the predicted q dependence of the first cumulant: in linear chains, it is given by the power law $\Omega(q) \propto q^3$ for the intramolecular dynamics with hydrodynamic interaction, irrespective of solvent conditions.[10,13] Conversely, for diffusive motion, we have $\Omega(q) = Dq^2$, as derived by the dynamic structure factor in the $t \rightarrow \infty$ limit, $S(q,t) = \exp(-Dq^2t)$. Here the diffusion coefficient is $D = k_BT/6\pi\eta_0R_H$, where R_H is the hydrodynamic radius (we calculated it for dendrimers in paper I). In the $t \rightarrow 0$ limit, we expect a similar result, due to the single-bead diffusion before it experiences the intramolecular forces due to connectivity: $S(q,t) = S(q, 0) \exp(-D_{bead}q^2t)$, where $D_{bead} = k_BT/\zeta$. Therefore, linear chains show a constant plateau in the $\Omega(q)/q^3$ plot for $q\langle R_S^2\rangle^{1/2} \gtrsim 1$.

On the other hand, branched molecules show a minimum of $\Omega(q)/q^3$ in this q range, as predicted[18] and observed[24] in star polymers. This minimum is expected to be much deeper in hyperbranched molecules such as dendrimers,[5] the more so the larger is their generation. Interestingly, it should take place at $q\langle R_S^2\rangle^{1/2} \approx 2$, essentially the same position as the maximum in the Kratky plot discussed in the previous Section. This fact shows their common origin in the large bead density due to the molecular topology. Furthermore, the curves of D1 and D2 phantom dendrimers are rather close to one another for a given g up to $q\langle R_S^2\rangle^{1/2} \approx 3 \div 4$ (see Figure 5, dashed curves). As discussed before for the Kratky plot, this is related to the same large-scale topology of the two dendrimer families, whose different local features become apparent at larger q. Once again, the similarity between D1 and D2 dendrimers in a good solvent breaks down because of the different expansion pattern.

The effect of good-solvent expansion is quite pronounced, resulting in any case in shallower minima and in a marked broadening and shifting of the maximum at larger $q\langle R_S^2\rangle^{1/2}$ for dendrimers with the largest g, once more in qualitative agreement with results for stiffer models.[5] The first feature is similar to the analogous broadening of the maximum in the Kratky plots shown in Figure 3. Also, for each dendrimer family the curves of $\Omega(q)/q^3$ at different g show a smaller vertical spread than in phantom molecules.

Turning now to the preaveraging approximation, we see from Figure 5 that it leads to a sizable error both in the position of the minimum of $\Omega(q)/q^3$, which is shifted to a slightly larger abscissa, and in its depth, which is somewhat enhanced. The amount of the error due to preaveraging can be clearly assessed through Figure 6, where we report the ratio $\Omega_{exact}(q)/\Omega_{preav}(q)$ as a function of $q\langle R_S^2\rangle^{1/2}$, with "exact" referring to the nonpreaveraged case. In all cases, we find $\Omega_{exact}(q)/\Omega_{preav}(q) > 1$, so that preaveraging amounts to systematically underestimate the first cumulant, hence also the time decay of the dynamic structure factor. In turn, this means that the intramolecular relaxation is somewhat faster than predicted through the preaveraging approximation. The latter conclusion also implies that the intrinsic viscosity $[\eta]$ must be less than calculated by this approximation, a result which agrees with computer simulations on both linear and star polymers,[25,26] and on dendrimers.[7] In fact, preaveraging amounts to using the average and not the instantaneous conformations, ignoring in particular the possibility of very close beads producing a large hydrodynamic interaction and in turn a fast loss of memory.

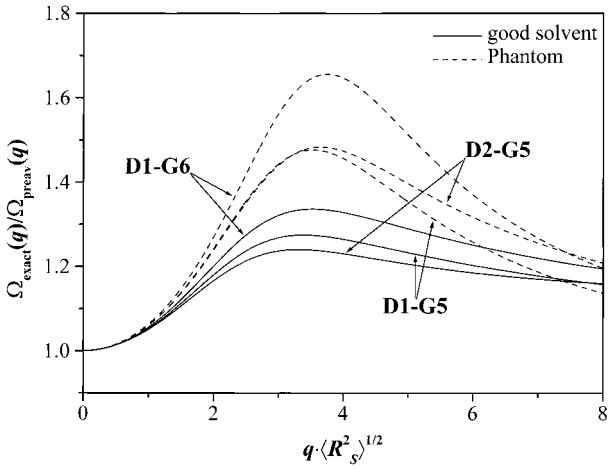

Figure 6. Relative error in the first cumulant due to preaveraging shown through $\Omega_{exact}(q)/\Omega_{preav}(q)$ plotted vs $q\langle R_S^2\rangle^{1/2}$ for the same dendrimers as in Figures 4 and 5.

Remarkably, the largest error due to preaveraging takes place in the range $2 < q\langle R_S^2\rangle^{1/2} < 4$. Moreover, it increases with dendrimer generation and is most severe in D1 dendrimers. This is in keeping with the notion that the preaveraging approximation becomes increasingly inaccurate with a larger local density due for instance to branching.[25,26] In fact, as shown in Figure 6, the error strongly decreases in a good solvent, in particular for the more open dendrimer D2. Clearly, intramolecular swelling brings the beads farther apart, in particular the branch points of D2 dendrimers, therefore making preaveraging a much better approximation, as already observed in computer simulations of linear and star polymers either with an increasing stiffness[25] or under good-solvent expansion.[26]

Concluding Remarks

In the present paper, we report our theoretical study of the intramolecular dynamics of dendrimers in a good-solvent. Using the Rouse−Zimm model with partial draining and exploiting the preaveraging approximation, we calculate the spectrum of relaxation times, the frequency-dependent complex modulus, and the dynamic structure factor. The latter quantity is characterized through its first cumulant, that shows analogies with the static structure factor.

The first cumulant may also be calculated without preaveraging the hydrodynamic interaction, and therefore it lends itself to estimate the accuracy of this approximation. We show that preaveraging leads to a nonnegligible error for most values of the scattering vector, but also that the error is strongly reduced under good-solvent expansion because of the lower local density of segments. Therefore, the smallest error is shown by the less-crowded D2 dendrimers that have two segments between adjacent branch points and undergo the largest excluded-volume expansion.

An important outcome of the present study is the qualitative similarity between the results obtained under good-solvent conditions and those obtained with stiff models. In fact, good-solvent expansion leads to an outward stretching of the dendra, with a correlation among the bond vectors that is largest near the central core. An essentially similar pattern can be achieved using ad hoc stiff (free-rotating) models with a larger persistence length in the core region, and a smaller one in the periphery.[5] Obviously such procedure does not

allow for a quantitative study of good-solvent effects over a family of dendrimers with different generations, i.e., the investigation carried out in paper I. The comparison between good-solvent expansion and local stiffness turns out to be appropriate for dendrimers because of the finite (and relatively small) generation they can achieve, due to the outer steric congestion, so that the two procedures indeed yield pretty similar results. On the other hand, in linear and star polymers this similarity must eventually break down, because stiffness may relieve the self-intersection problem on the local scale, but not on the large scale when the contour length is much larger than the persistence length. Conversely, bond correlation due to good-solvent expansion accounts also for the large-scale interactions, thus being asymptotically much different.

Appendix

The purpose of this appendix is to give a more general description of the degeneracy of the eigenvalues in dendrimers than that given in ref 6. Hydrodynamic interaction and good-solvent expansion, here ignored, do not alter the degeneracies, but may modify the ordering of the eigenvalues, as well as the eigenvectors, defined here using the bead positions as the dynamical variables (see eq 2). The eigenvalues can be nondegenerate or can have a degeneracy larger than 1 according to molecular symmetry, and the degenerate eigenvalues can be collected in different subgroups.[6] The number P of segments between adjacent branch points does not change the symmetry, hence the degeneracy, but it does change the *number* of subgroups. Let us define a shell as a set of beads at the same topological distance from the core. A DP dendrimer has $1 + (g + 1)P$ shells, numbered from 0 (the core) up to $(g + 1)P$. The branch points belong to shells jP, $j = 0, 1, 2, ..., g$ (including the core for $j = 0$).

The eigenvalues can be grouped into three major sets:

(1) One zero eigenvalue, related to molecular diffusion.

(2) $(g + 1)P$ nondegenerate eigenvalues (the associated eigenvectors have no nodes at the branch point and the $(g + 1)P$ shells move in phase).

(3) $n - (g + 1)P - 1$ degenerate eigenvalues, divided in different subgroups.

We now list the degeneracies within each subgroup of the third set, which depend on the number of nodes of the associated eigenvector:

(a) $(g + 1)P$ subgroups of eigenvalues with an $f - 1$ degeneracy; the eigenvectors have a single node at the core and span the $(g + 1)P$ shells from 1 to $(g + 1)P$, so that all external shells move in phase.

(b) $(g - k)P$ subgroups of eigenvalues with degeneracy $fm^k(m - 1)$, $k = 0, 1, 2, ..., g - 1$: the eigenvectors have zero values at the core and at the inner $(k + 1)P$ shells, and nonzero values at the outer $(g - k)P$ shells [from shell $(k + 1)P + 1$ to the terminal shell $(g + 1)P$].

Therefore, the degenerate eigenvalues of the third set are in total $(f - 1)(g + 1)P + (g-k)Pfm^k(m-1) = \mathrm{P}(f[m^{g+1} - 1]/[m - 1] - g - 1)$. Together with the $(g + 1)P + 1$ nondegenerate eigenvalues of the first two sets, they give a total of $n = 1 + fP(m^{g+1} - 1)/(m - 1)$ eigenvalues, as required.

Acknowledgment. We gratefully thank Professor G. Allegra for useful discussions. We acknowledge the financial support by CNR (Consiglio Nazionale delle Ricerche, Italy) Project "Materiali Speciali per Tecnologie Avanzate II", and by MURST (Ministry of University and of Scientific and Technological Research, Italy).

References and Notes

(1) Tomalia, D. A.; Naylor, A. M.; Goddard, W. A., III. *Angew. Chem., Int. Ed. Engl.* **1990**, *29*, 138.
(2) Bosman, A. W.; Janssen, H. M.; Meijer, E. W. *Chem. Rev.* **1999**, *99*, 1665.
(3) Tomalia, D. A.; Baker, H.; Dewald, J. R.; Hall, M.; Kallos, G.; Martin, S.; Roeck, J.: Ryder, J.; Smith, P. *Polym. J. (Tokyo)* **1985**, *17*, 117. Newkome, G. R.; Yao, Z.; Baker, G. R.; Gupta, V. K. *J. Org. Chem.* **1985**, *50*, 2003. Hawker, G.; Fréchet, J. M. J. *J. Chem. Soc., Chem. Commun.* **1990**, 1010.
(4) Ganazzoli, F.; La Ferla, R.; Terragni, G. *Macromolecules* **2000**, *33*, 6611.
(5) La Ferla, R. *J. Chem. Phys.* **1997**, *106*, 688.
(6) Cai, C.; Chen, Z. Y. *Macromolecules* **1997**, *30*, 5104.
(7) Cai, C.; Chen, Z. Y. *Macromolecules* **1998**, *31*, 6393. Chen, Z. Y.; Cai, C. *Macromolecules* **1999**, *32*, 5423.
(8) Mansfield, M. L.; Klushin, L. I. *J. Phys. Chem.* **1992**, *96*, 3994.
(9) Zimm, B. H. *J. Chem. Phys.* **1956**, *24*, 269.
(10) Doi, M.; Edwards, S. F. *The Theory of Polymer Dynamics*; Oxford Scientific Publications: Oxford, England, 1986.
(11) Bixon, M. *J. Chem. Phys.* **1973**, *58*, 1459. Zwanzig, R. *J. Chem. Phys.* **1974**, *60*, 2717.
(12) Perico, A. *Acc. Chem. Res.* **1989**, *22*, 336.
(13) Allegra, G.; Ganazzoli, F. *Adv. Chem. Phys.* **1989**, *75*, 265.
(14) Ganazzoli, F.; Allegra, G.: Colombo. E.; De Vitis, M. *Macromolecules* **1995**, *28*, 1076.
(15) Akcasu, A. Z.; Gurol, H. *J. Polym. Sci. B* **1976**, *14*, 1.
(16) Technically, this means that the parameter for the repulsive two-body interactions among the beads was chosen as $\tau B = 0.5$ (see Figures 2, 3, 6, 8, and 9 of ref 4).
(17) Ganazzoli, F. *J. Chem. Phys.* **1997**, *106*, 8913.
(18) Burchard, W. *Adv. Polym. Sci.* **1983**, *48*, 1.
(19) Kirste, H. G.; Oberthür, R. C. In *Small Angle X-ray Scattering*; Glatter, O., Kratky, O., Eds.; Academic Press: London, 1982; p 387.
(20) Mansfield, M. L.; Klushin, L. I. *Macromolecules* **1993**, *26*, 4262.
(21) Scherrenberg, R.; Coussens, B.; van Vliet, P.; Edouard, G.; Brackman, J.; de Brabander, E.; Mortensen, K. *Macromolecules* **1998**, *31*, 456.
(22) Prosa, T. J.; Bauer, B. J.; Amis, E. J.; Tomalia, D. A.; Scherrenberg, R. *J. Polym. Sci. B: Polym. Phys.* **1997**, *35*, 2913.
(23) Ganazzoli, F.; Kuznetsov, Yu. A.; Timoshenko, E. G. *Macromol. Theory Simul.*, in press.
(24) Richter, D.; Farago, B.; Fetters, L. J.; Huang, J. S.; Ewen, B. *Macromolecules* **1990**, *23*, 1845.
(25) Zimm, B. H. *Macromolecules* **1980**, *13*, 592; **1984**, *17*, 795.
(26) Freire, J. J.; Rey, A.; Bishop, M.; Clarke, J. H. R. *Macromolecules* **1991**, *24*, 6494.

MA001613Z